M. de Pontes, R.L. Espinoza, C.P. Nicolaides, J.H. Scholz and M.S. Scurrell (Editors)
Natural Gas Conversion IV
Studies in Surface Science and Catalysis, Vol. 107

© 1997 Elsevier Science B.V. All rights reserved.

Fischer-Tropsch Synthesis on Cobalt Catalysts: Structural Requirements and Reaction Pathways

Enrique Iglesia, Department of Chemical Engineering, University of California at Berkeley, Berkeley, CA 94720, USA.

Abstract

Fischer-Tropsch synthesis turnover rates on supported Co catalysts are independent of Co dispersion and of support identity over the accessible dispersion range (0.01-0.12). Turnover rates increase when small amounts of Ru (Ru/Co<0.008 at.) are added to Co catalysts. Co dispersions above 0.15 lead to rapid deactivation during reaction. Optimum dispersions (0.10-0.15) can be achieved, even at high Co loadings, by slow reduction of supported Co nitrate precursors. C_5+ selectivity increases with increasing Co site density because diffusion-enhanced readsorption of α-olefins reverses β-hydrogen abstraction chain termination steps. Severe diffusional restrictions, however, can also deplete CO within catalyst pellets and decrease chain growth probability. Therefore, high C_5+ selectivities are obtained on catalysts with moderate diffusional restrictions. Diffusional constraints depend on pellet size and porosity and on the density and radial location of Co sites within catalyst pellets. The support pore structure and pellet size and the intrapellet distribution and density of Co sites can be used to design supported Co catalysts with high C_5+ selectivity and reaction rates.

1. Introduction

The Fischer-Tropsch synthesis (FTS) is a polymerization reaction that uses CH_x monomers derived from synthesis gas to form high molecular weight hydrocarbons. Recent advances in the design and use of slurry reactors [1-3] have increased the economic incentives for its industrial practice. These new reactors have also restored the scientific importance of the underlying kinetic processes by lessening the severe heat and mass transfer restrictions ubiquitous in packed-bed reactors.

Chain growth occurs by addition of surface methylene species to adsorbed alkyl groups, which terminate to form predominantly linear α-olefins (by β-hydrogen abstraction) and n-paraffins (by hydrogen addition) on Co catalysts [4,5]. Chain growth kinetics often depend on chain size, leading to non-Flory carbon number distributions in FTS products [6-12]. This review describes the effects of crystallite size, support, and alloying on the turnover rate and selectivity of supported Co catalysts. It also explores subtle secondary reactions and diffusional restrictions, which influence FTS selectivity and introduce catalyst design parameters unavailable in kinetic-limited catalysts. The details of the experimental and simulation methods have been reported previously [9-16].

2. Cobalt Dispersion and Support Effects

The design of Co catalysts with high specific rates has focused on synthetic methods to decrease metal crystallite size and on the use of supports that may increase the

rate per surface Co atom (turnover rate). Early studies of CO hydrogenation to form light paraffins detected strong effects of crystallite size on turnover rate [17]. Surface Co atoms in small crystallites were be less active for FTS reactions. Later studies showed that incomplete reduction of CoO_x precursors and re-oxidation of Co during FTS cause this apparent structure sensitivity [18]. Similarly, TiO_2 supports lead to higher methanation turnover rates on several metals [19] because TiO_x overlayers form during reduction influence CO and H_2 adsorption. These overlayers, however, are rapidly reversed by water formed during FTS reactions at useful synthesis gas pressures and conversions [9,14].

At conditions favoring chain growth (C_5+ selectivity > 80%), FTS rates per (total) Co atom increase linearly with increasing Co dispersion, irrespective of the chemical identity of the underlying support (Figure 1), over the experimental dispersion range (0-0.12). Thus, turnover rates are not influenced by dispersion or support effects. These results are reassuring because crystallite surface structure and orientation (and thus turnover rates) should depend weakly on crystallite diameter over the experimental Co dispersion range [20,21]. Recent studies have shown that methanation turnover rates are also independent of Co dispersion on supported catalysts [18,22] and of surface orientation on Co single crystals and films [18,23].

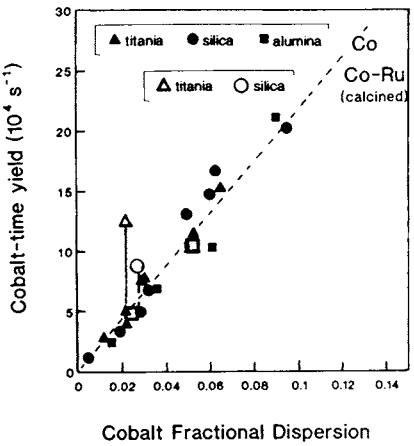

Figure 1. Effect of cobalt dispersion (ratio of surface Co to total Co atoms), support, and alloying on FTS Co-time yields (mole CO converted/total g-atom Co-s) [Reaction conditions: 473 K, 2000 kPa, H_2/CO=2.05, C_5+ selectivity > 80%; 0.17 mm pellet size]

Table 1. Pretreatment effects on Co dispersion [13%wt. Co/SiO_2, impregnated to incipient wetness with Co nitrate solution]

Treatment	Co Dispersion from hydrogen chemisorption
Air (673 K); H_2 (to 623 K at 4 K min^{-1})	0.030
H_2 (to 623 K at 4 K min^{-1})	0.057
H_2 (to 623 K at 0.2 K min^{-1})	0.118

Co dispersions above 0.10 can be achieved by using carbonyl precursors or by impregnation with concentrated nitrate solutions followed by direct reduction of nitrate precursors (Table 1) [16]. Small Co crystallites require strong interactions between the support and the Co precursor, which interfere with the reduction of such precursors to Co metal at low temperatures [24]. On strongly interacting supports, the high reduction temperatures required lead to sintering. Optimum Co dispersions are obtained using

support-precursor combinations with intermediate interaction strength [24]. For example, alumina-nitrate and silica-carboxylate combinations lead to very small CoO_x particles, which reduce completely only above 800 K. Silica-nitrate and $MgCr_2O_4$-nitrate pairs lead to CoO_x particles of intermediate size during nitrate decomposition; these crystallites reduce at 573-673 K without significant agglomeration.

Exothermic oxidation of nitrate precursors during calcination and high H_2O partial pressures during reduction deleteriously affect metal dispersion. As a result, direct reduction of nitrate precursors at high H_2 flow rates using slow temperature ramps lead to Co dispersions above 0.10 (Table 1) even at high Co concentrations, such as those required in eggshell catalyst configurations [16]. Co metal crystallites smaller than about 5-6 nm (0.15-0.2 dispersion), however, appear to re-oxidize at typical FTS reaction conditions. Thus, it is unlikely that marked improvements in volumetric productivities can be achieved solely by increasing Co metal dispersions above 0.15. Catalyst productivities, however, can be increased by preparing catalysts via synthetic methods that maintain dispersions near 0.15 even at high Co loadings. These Co dispersions can be achieved by the use of appropriate support-precursor combinations and by the controlled reduction of the impregnated precursors. These techniques lead to very high volumetric Co site densities, which, as we discuss below, favor high selectivity to desired C_5+ products.

3. Structural and Chemical Promotion of Cobalt by Other Metals

Catalyst productivity in FTS reactions can also be increased by combining Co with another metal in order to increase the number of exposed Co sites (structural promotion) or the FTS rate per exposed Co metal atom (chemical promotion). Structural promotion occurs when the alloying element increases Co dispersion by modifying the strength of CoO_x-support interactions or the reducibility of CoO_x. Ru lowers the reduction temperature of CoO_x supported on Al_2O_3, SiO_2, and TiO_2 [15]; on Al_2O_3, the presence of Ru leads to higher apparent metal dispersions and more complete reduction, as also reported by others [25]. Re appears to prevent CoO_x agglomeration during calcination treatments and oxidative regeneration [26-28]; Re leads to higher Co metal dispersions on TiO_2 without influencing FTS turnover rates. The presence of Re (0.8% wt.) in Co/TiO_2 leads to an increase in dispersion from 0.022 to 0.053 (Figure 1, open squares), apparently by forming Re oxide species that anchor CoO_x clusters and inhibit sintering under oxidizing conditions.

Alloying elements can also act as chemical promoters and increase reaction turnover rates. Ru increases FTS turnover rates on Co/SiO_2 and Co/TiO_2 catalysts (Figure 1) [15]. The presence of very small amounts of Ru (Ru/Co=0.0067 at., 11.7% Co/TiO_2; 0.022 dispersion) increases turnover rates from 1.7×10^{-3} s^{-1} to 5.6×10^{-3} s^{-1}, without an apparent increase in Co dispersion (Figure 1). This synergistic effect is enhanced by improved bimetallic mixing, induced by oxidation above 573 K and detected by in-situ X-ray absorption measurements [15]. The observed increase in turnover rates cannot be explained by the FTS activity of Ru atoms, even if all Ru atoms resided at Co crystallite surfaces. The presence of Ru does not influence FTS reaction rate orders or activation energies. Ru appears to preserve a larger fraction of the surface Co atoms active during FTS reactions. This inhibition of deactivation processes in Co-Ru bimetallic catalysts is consistent with independent thermogravimetric data and X-ray photoelectron spectra,

which show that carbon deposition from H_2/CO occurs at higher temperatures when Ru is added to Co/TiO_2 catalysts [15]. Re-oxidation of surface Co atoms in small crystallites may also be influenced by the presence of a noble metal. This inhibited oxidation of Co alloys containing noble metals may increase the stability of cobalt catalysts against oxidation during FTS, especially for small crystallites at typical high conversion conditions in backmixed slurry reactors.

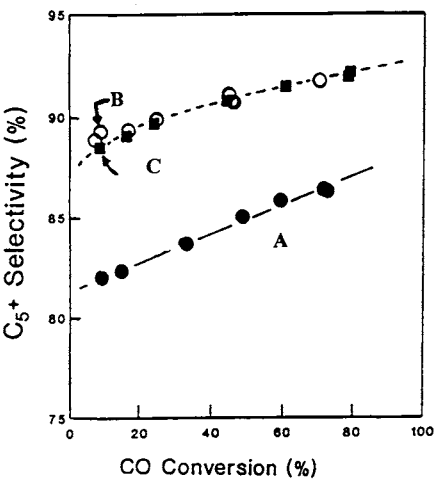

Figure 2. Site density and alloy effects on C_5+ selectivity (Co/TiO_2) [**A**: 11.7% Co, 0.022 dispersion (d), 10^{-6} g-atom surface Co m^{-2} (θ_{Co}); **B**: 12.1% Co, d=0.058, θ_{Co}= 3.3 x 10^{-6}; **C**: 11.7% Co, $(Ru/Co)_{at}$ = 0.0067, d=0.024, θ_{Co}= 1.1 x 10^{-6}] [0.17 mm pellet size; reaction conditions as in Figure 1]

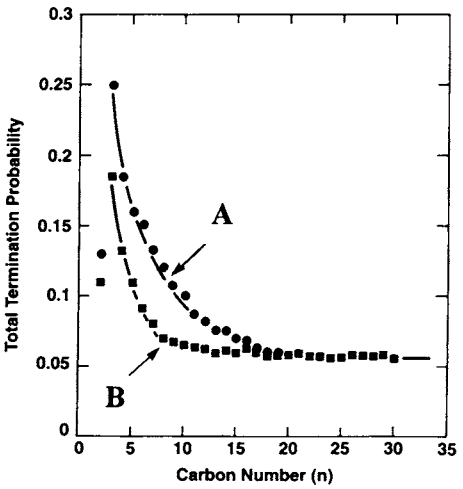

Figure 3. Bed residence time and carbon number effects on chain termination probability. **A:** 9.5% CO conversion, 2 s bed residence time; **B:** 72% CO conversion, 12 s bed residence time [Co/TiO_2, 11.7% Co, 0.015 dispersion, 0.17 mm pellet size; 473 K, 2000 kPa, H_2/CO=2.1]

4. Structural and Compositional Effects on Selectivity

FTS selectivity is influenced by the structure and composition of Co crystallites and of the metal oxide support, suggesting an unexpected structure sensitivity of FTS chain growth reactions on Co [9]. For example, increasing the Co dispersion of Co/TiO_2 from 0.022 to 0.06 increases C_5+ selectivity from 85% to 90.5% (Figure 2; 50% conversion). A similar increase in C_5+ selectivity is caused by the addition of Ru (Figure 2), which increases apparent turnover rates by a factor of three without influencing the initial Co metal dispersion (Figure 1). Figure 2 also shows an increase in C_5+ selectivity as conversion is increased by increasing reactor residence time. This increase in C_5+ selectivity is accompanied by lower CH_4 selectivity and C_2-C_{15} chain termination probabilities, without any influence on the growth rates for C_{15+} chains (Figure 3). Chain termination appears to be reversed by increasing residence time and to become less likely for larger chains (Figure 3). This latter effect leads to the non-Flory molecular weight distributions widely reported in the FTS literature [4,9,13].

4.1 Chain Termination and α-Olefin Readsorption

The readsorption of α-olefins can decrease the termination probability of growing chains by reversing the predominant β-hydrogen abstraction termination step. This well-known secondary reaction leads to an increase in C_5+ selectivity and to lower CH_4 and olefin contents within reaction products. Its effect on FTS selectivity becomes stronger as olefin concentrations increase with increasing bed residence time and CO conversion. Bed residence time studies have shown that α-olefins initiate surface chains with very high selectivity during FTS [4,9], even though α-olefins added to H_2/CO feeds undergo significant hydrogenation (Table 2), especially at low CO pressures or conversions. The water formed in FTS steps strongly inhibits olefin hydrogenation; thus added olefins hydrogenate predominantly at the dry conditions of the reactor inlet. The addition of water with the H_2/CO feed or the introduction of olefins below the reactor inlet markedly increase the chain initiation selectivity (Table 2). Previous studies of secondary reactions using olefin addition to H_2/CO feeds have markedly underestimated their critical role in the control of selectivity during FTS reactions.

Table 2. Hydrogenation and chain initiation reactions of ethylene during FTS [11.7% Co/TiO_2, 0.017 dispersion, 2070 kPa, <15% CO conversion, 8% mol. C_2H_4 in feed, H_2/CO=2.1] [9]

Ethylene Source	Hydrogenation (%)	Chain Initiation (%)
added (at inlet) with H_2/CO	70.5	29.5
formed from H_2/CO during FTS	15.1	84.9
added (below inlet) with H_2/CO	31.5	68.5
added (at inlet) with 15% H_2O-H_2/CO	22.0	78.0

4.2 Diffusion-Enhanced Chain Growth by α-Olefin Readsorption and Site Density Effects on Selectivity.

Termination probabilities for each hydrocarbon size (β_n, Figure 3) can be calculated from the complete molecular weight distribution and separated into olefin and paraffin termination steps for each carbon number (Scheme, Figure 4). The decrease in chain termination probability observed as chain size increases reflects a decrease in the net rate of the reversible termination to olefins, without any apparent influence of chain size on the irreversible H-addition termination step that forms paraffins (Figure 4). Therefore, chain size should also not strongly influence the intrinsic forward rate of β-hydrogen abstraction steps that lead to chain termination to α-olefins. The observed decrease in the *net* olefin termination probability reflects the higher probability of reversal by readsorption as chain size increases. This higher probability in turn reflects the slower diffusivity and the generally higher reactivity of larger olefins, which increase the severity of diffusional restrictions within liquid-filled pores [9].

Rigorous mathematical descriptions of diffusional transport within catalyst pellets and of chain growth and termination surface kinetics lead to excellent agreement with experimental measurements of chain termination probabilities. For example, the curves shown in Figure 4 were obtained from simulations using these models [9,13] and:

$$(D_n / k_{r,n}) = (D_6 / k_{r,6}) \exp [-\gamma (n-6)] \qquad (1)$$

in order to describe the diffusivity (D_n) and reactivity ($k_{r,n}$) of olefins with n carbons using the values for 1-hexene and a value of γ adjusted to match the data in Figure 4 (γ= 0.29). This exponential dependence includes chain size effects on olefin diffusivity and reactivity.

Scheme. Chain Growth Pathways in Fischer-Tropsch Synthesis on Co

$\beta_{T,n} = r_{t,n} / r_{p,n} = \phi_n / \Sigma^{\infty}_{n+1} \phi_i$

$\beta_{T,n} = \beta_{o,n} + \beta_{T,n} + \beta_{T,n}$

ϕ_n = molar rate of formation of chains with n carbons

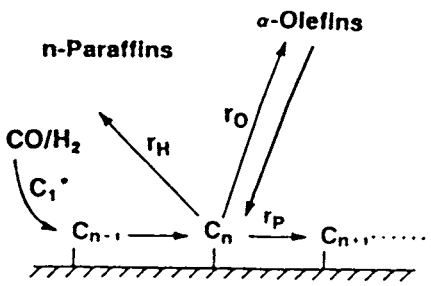

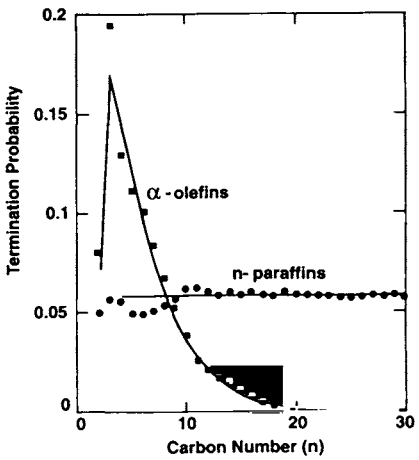

Figure 4. Bed residence time and carbon number effects on chain termination probabilities to olefins and paraffins [9.5% CO conversion, 2 s bed residence time; Co/TiO_2, 11.7% Co, 0.015 dispersion, 0.17 mm pellet size; 473 K, 2000 kPa, H_2/CO=2.1]

Dimensional analysis of this reaction-transport model shows that the effect of diffusional restrictions on readsorption rate is controlled by a dimensionless parameter Φ_n :

$$\Phi_n = (k_{r,n} / D_n) \times (R_o^2 \varepsilon \theta_{Co} / r_p) = (\psi_n) \times (\chi) , \qquad (2)$$

which reflects the ratio of maximum diffusion rates to maximum reaction rates for olefins with n carbons. The first term (ψ_n) in Equation (2) contains the rate constant for the first-order olefin readsorption turnover rate ($k_{r,n}$) and the effective diffusivity (D_n) of α-olefins within support pellets. This term reflects the molecular properties of olefins of a given size

and leads to the observed effect of carbon number on chain termination probability and on olefin content (Figures 3 and 4).

The second term (χ) contains the pellet radius (R_o), the density of Co sites per unit area (θ_{Co}), and the support void fraction (ε) and average pore radius (r_p). The last three catalyst properties appear as a combined term ($\varepsilon\theta_{Co}/r_p$) that is proportional to the number of Co sites per unit pellet volume. The χ term depends on the structural properties of the catalyst support and on the number of surface Co atoms involved in the formation and readsorption of olefins. This term accounts for the observed increase in the extent of readsorption and in C_5+ selectivity as Co site density is increased either by increasing the Co loading or dispersion in monometallic catalysts or by maintaining a larger fraction of the exposed Co surface atoms available during FTS in Co-Ru catalysts (Figure 2). In both cases, chain termination probabilities decrease as site density increases because termination to olefins is selectively reversed by readsorption without modifying the rate of chain termination to paraffins. This last step determines asymptotic chain termination probabilities for C_{15}+ paraffins. Therefore, chain termination probabilities for C_{15}+ products are not influenced by Co site density or support structure.

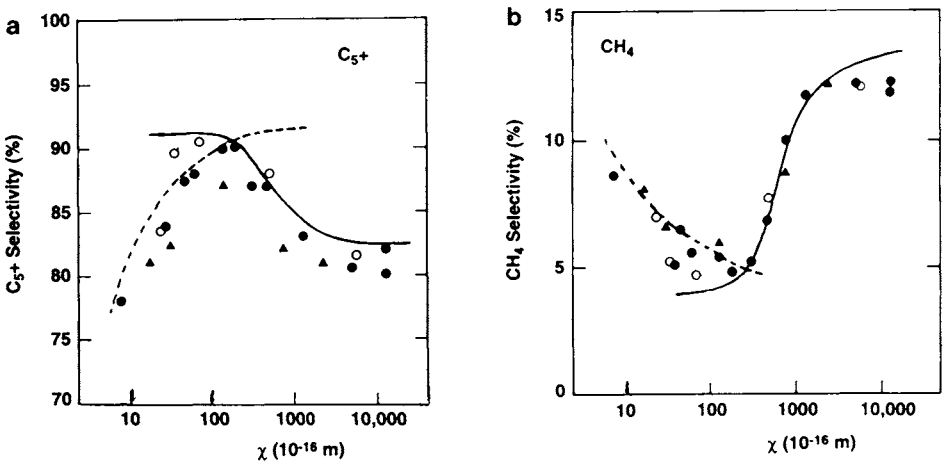

Figure 5. The effect of structural parameters (χ) on FTS selectivity: Diffusion-enhanced readsorption (- - - -) and diffusion-inhibited chain growth (——) simulations and experimental data (● , dispersion/support effects; ▲ , pellet size variations; o , eggshell thickness variations: a) C_5+ selectivity; b) CH_4 selectivity [473 K, 2000 kPa, H_2/CO = 2.1, 55-65 % CO conversion] *(χ values from Equation 2, with r_p and R_o in m and θ_{Co} in surface Co atoms m^{-2})[9,16]*

C_5+ selectivity increases (Figure 5a) and CH_4 selectivity decreases (Figure 5b) as the value of the structural parameter (χ) increases, suggesting that more severe transport restrictions increase the probability of chain growth. The broken curves in Figure 5 represent model simulations in which the effect of catalyst structure is described using identical values of olefin diffusivities and of chain growth and readsorption rate constants for all catalysts. Differences in selectivity caused by alloying or by changes in the support identity or the Co dispersion reflect the indirect effect of these properties on diffusion-

enhanced readsorption reactions. Dispersion, support, and bimetallic effects do not influence the intrinsic chain growth properties of Co surfaces in the experimental dispersion range. Excellent agreement between experiments and simulations can be obtained without varying the nature of the surface chain growth kinetics. Thus, intrinsic chain termination kinetics need not depend on carbon number in order to explain non-Flory carbon number distributions (Figure 4) or the observed effect of site density and pore structure on carbon number and olefin selectivities (Figure 5).

Recently, non-Flory distributions have been attributed to the higher solubility of larger α-olefins in FTS liquid products [29-31]. These authors correctly state that vapor-liquid equilibrium favors the presence of larger olefins in FTS liquids, but incorrectly conclude that such higher concentrations lead to higher kinetic readsorption rates. Chemical reactions are driven by changes in a thermodynamic property called the chemical potential, which is identical for a given component in two or more phases that co-exist in thermodynamic equilibrium. Olefin readsorption rates depend only on the olefin thermodynamic activity (not its concentration), which at vapor-liquid equilibrium is identical in the liquid and gas phases and independent of solubility at steady-state. A chemical reaction cannot "detect" the presence of a liquid phase unless the liquid phase introduces either a transport restriction or a change in the reactive properties of the catalytic surface. Solubility-enhanced olefin readsorption, even if consistent with thermodynamics, cannot account for the observed effects of site density and pellet size on selectivity, because neither variable influences vapor-liquid equilibrium properties.

4.3 Diffusion-Inhibited Chain Growth

The selectivity trends caused by diffusion-enhanced olefin readsorption are ultimately reversed as transport restrictions become more severe ($\chi > 200 \times 10^{16}$ m^{-1}) (Figure 5). Large pellets and high Co site densities lead to an apparent inhibition of chain growth because severe transport restrictions lead to CO depletion within intrapellet liquids. CO activity gradients lead to lower chain propagation rates and to low chain growth probability. In this case, chain termination probabilities (r_t/r_p) increase because diffusional restrictions inhibit chain growth. CO diffusional restrictions depend on a dimensionless parameter that accounts for the relative rates of CO diffusion and CO hydrogenation:

$$\Phi_{CO} = (\psi_{CO}) \times (R_o^2 \; \varepsilon \; \theta_{Co} / r_p) = (\psi_{CO}) \times (\chi) , \qquad (3)$$

where ψ_{CO} is a function of the rate constant for CO hydrogenation and of the CO diffusivity and χ is identical to the structural parameter derived from the readsorption model. The solid curves in Figures 5a and 5b show the result of simulations using CO hydrogenation rate expressions obtained in kinetic-limited measurements and independently measured values for the H_2 and CO diffusivities and solubilities in FTS liquid products [9,13,16]. These simulations are in excellent agreement with the experimental results. Fortunately, the onset of CO transport restrictions occurs for χ values much higher than those required to enhance chain growth, because CO diffuses through intrapellet liquids more rapidly than olefins ($\psi_{CO} << \psi_n$). Very few olefins remain in the product stream for χ values leading to maximum C_5+ selectivities, suggesting that

the full benefit of olefin readsorption can be extracted before CO depletion starts to inhibit chain growth.

4.4 Optimum C_5+ Selectivity and Catalyst Design in the Fischer-Tropsch Synthesis

Optimum FTS selectivities (> 90%) are achieved on catalysts with intermediate χ values. The physical structure and the Co site density in FTS catalysts can be designed and constructed in a way that leads to the desired carbon number distribution and olefin content in products. None of these design variables influence the selectivity in kinetic-limited catalyst pellets. Light olefins are favored at very low χ values and light paraffins are formed preferentially at very high values of χ. Intermediate χ values lead to heavy paraffins and minimize the formation of light products.

Reactor and economic constraints determine the range of volumetric site densities (productivity) and pellet size (pressure drop in packed beds). These considerations may limit the range of χ values that can be achieved using uniformly impregnated pellets. In such instances, the use of pellets with Co sites preferentially located near the outer pellet surface allows the characteristic diffusion length to be varied independently of pellet diameter [16,32,33]. The relevant structural factor for such eggshell pellets becomes:

$$\chi = (\delta_o^2 \varepsilon \theta_{Co} / r_p), \qquad (4)$$

where δ_o is the thickness of the eggshell layer [9,16]. The open symbols included in Figure 5 illustrate the remarkable flexibility introduced by eggshell configurations in the design of FTS catalysts. The open symbol to the extreme right corresponds to a uniformly impregnated large SiO_2 pellet (2.2 mm diameter); the right to left sequence of open symbols shows how decreasing the eggshell thickness within such pellets markedly increases C_5+ selectivity and minimizes the selectivity to CH_4 [9,16] without a significant decrease in volumetric catalyst productivity. The latter can be achieved, in spite of the much smaller support volume and surface area onto which Co sites must be introduced, by using precursor-support pairs with intermediate interaction strength and by the slow reduction of Co nitrate precursors. Slow reduction of nitrate precursors on SiO_2 leads to Co dispersions above 0.08 even at 50% wt. local Co loadings [16].

Eggshell catalysts are useful in packed-bed reactors, in which volumetric productivity and pressure drop constraints require the use of pellets with high χ values. In slurry reactors, catalyst particles are much smaller and χ is often lower than optimum values. Higher values of χ require the selective deposition of Co sites near the pellet center or a significant increase in the site density and volumetric productivity of catalyst pellets. The latter approach is preferred because it also increases reactor productivity; it requires, however, the synthesis of high-loading supported Co catalysts with high Co dispersion (>10%). Slurry liquids that inhibit olefin diffusion increase values of ψ_n (Equation 2) and can be used to compensate for the low values of χ typical of small catalyst particles in slurry reactors.

5. Acknowledgments

This manuscript is based on a plenary lecture delivered at the 4th International Natural Gas Conversion Symposium. The results described in this review were obtained

in collaborations with Stuart L. Soled, Sebastian C. Reyes, Joseph E. Baumgartner, Rostam J. Madon, and Rocco A. Fiato at the Corporate Research Laboratory of Exxon Research and Engineering Co.

6. References

1. Kolbel, H. and Ralek, M., Catal. Rev. 21 (1980) 225.
2. Jager, B., Kelfkens, R.C., Steynberg, A.P., Stud. Surf. Sci. Catal. 81 (1994) 419.
3. Bhatt, B.L., Frame, R., Hoek, A., Kinnari, K., Rao, V.U.S., and Tungate, F.L., Topics in Catalysis 2 (1995) 235.
4 Biloen, P., Helle, J.N., and Sachtler, W.M.H., J. Catal. 58 (1979) 58.
5. Brady, R.C. and Pettit, R., J. Am. Chem. Soc. 103 (1981) 1287.
6. Pichler, H., Schulz, H., and Elstner, M., Brennst. Chem. 48 (1967) 78.
7. Schulz, H., Beck, K., and Erich, E., Proc. 9th Int. Congr. Catal. 2 (1988) 829.
8. Vanhove, D., Zhuyong, Z., Makambo, L., Blachard, M., Appl. Catal. 9 (1984) 327.
9. Iglesia, E., Reyes, S.C., Madon, R.J., and Soled ,S.L., Adv. Catal. Rel. Subj. (D.D. Eley, H. Pines, P.B. Weisz, eds.) vol. 39, p. 239. Academic Press, 1993.
10. Iglesia, E., Reyes, S.C., and Madon, R.J., J. Catal. 129 (1991) 238.
11. Madon, R.J., Reyes, S.C., and Iglesia, E., ACS Symp. Ser. 517 (1992) 383.
12. Madon, R.J., Reyes, S.C., and Iglesia, E., J. Phys. Chem. 95 (1991) 7795.
13. Iglesia, E., Reyes, S.C., and Soled ,S.L., in Computer-Aided Design of Catalysts and Reactors (E.R. Becker, and C.J. Pereira, eds.) p. 199, Marcel Dekker, 1993.
14. Iglesia, E., Soled, S.L., and Fiato, R.A., J. Catal. 137, (1992) 212.
15. Iglesia, E., Soled, S.L., Fiato, R.A., and Via, G.H., J. Catal. 143 (1993) 345.
16. Iglesia, E., Soled, S.L., Baumgartner, J.E., and Reyes, S.C., J. Catal. 153 (1995).
17. Bartholomew, C.H. and Reuel, R.C., J. Catal. 85 (1984) 78.
18. Johnson, B.G., Bartholomew, C.H., and Goodman, D.W., J. Catal. 128 (1991) 231.
19. Vannice, M.A., Catal. Rev. 14 (1976) 153.
20. Boudart, M., Adv. Catal. Rel. Subj. 20 (1969) 85.
21. van Hardeveld, R. and Hartog , F., Adv. Catal. Rel. Subj. 22 (1972) 75.
22. Ho, S.W., Houalla, M., and Hercules, D.M., J. Phys. Chem. 94 (1990) 6396.
23. Geerlings, J.J.C., Zonnevylle, M.C., de Groot, C.P.M., Surf. Sci. 241 (1991) 302, 315.
24. Soled, S.L., Baumgartner, J.E., Reyes, S.C., and Iglesia, E., Proc. Mater. Res. Soc. Symp. 368, (1995) 113.
25. Beuther, H., Kibby, C.L., Kobylinski, T.P., Pannell, R.B., U.S. Pat. 4 413 064 (1983); 4 493 905 (1985); 4 585 798 (1986), assigned to Gulf Research and Development
26. Mauldin, C.H. and Riley, K.L., Eur. Patent Appl. 453 674 (1991), assigned to Exxon.
27. Eri, S., Goodwin J.G., Marcelin, G., Riis, T., U.S. Patent 4 801 573 (1989).
28. Vada, S., Hoff, A.,Adnanes, E., Schanke, D., and Holmen, A., Top. Cat. 2 (1995) 155.
29. Schulz, H., Beck, K., and Erich, E., Stud. Surf. Sci. Catal. 36 (1988) 457.
30. Tau, L.M., Dabbagh, H.A., and Davis, B.H., Catal. Lett. 7 (1990)127; Energy Fuels 4 (1990) 94.
31. Kuipers, E.W., Vinkenburg, I.H., and Oosterbeek, H., J. Catal. 152 (1995) 137.
32. van Erp, W.A., Nanne, J.M., and Post, M.F.M., U.S. Patent 4 637 993 (1987), assigned to Shell.
33. Mauldin, C.H. and Riley, K.L., U.S. Patent 4 977 126 (1990), assigned to Exxon.